International Journal of Biological Macromolecules 209 (2022) 1477–1485

Contents lists available at ScienceDirect

International Journal of Biological Macromolecules

journal homepage: www.elsevier.com/locate/ijbiomac

Synthesis and drug release properties of melanin added functional allopurinol incorporated starch-based biomaterials

Han-Seong Kim [a,1], Chang-Moon Lee [b,1], Yeon-Hum Yun [c,1], Youn-Sop Kim [a,*], Soon-Do Yoon [a,*]

[a] Department of Biomolecular and Chemical Engineering, Chonnam National University, Jeonnam 59626, South Korea
[b] Department of Biomedical Engineering, Chonnam National University, Yeosu, Jeonnam 59626, Republic of Korea
[c] Department of Energy & Resources Engineering, Chonnam National University, Gwangju 61186, Republic of Korea

ARTICLE INFO

Keywords:
Functional biomaterial
Allopurinol
Melanin
Photothermal conversion efficiency
Release properties

ABSTRACT

The main objective of this study was to prepare functional allopurinol (ALP) incorporated biomaterials using mungbean starch, polyvinyl alcohol, melanin (MEL), and plasticizers. Prepared biomaterials were characterized by FE-SEM and FT-IR analysis. Photothermal conversion efficiencies and ALP release properties of biomaterials were evaluated with NIR laser irradiation. When biomaterials were irradiated with the NIR laser, temperatures increase of MEL-added biomaterials were higher than those of MEL-non-added biomaterials. After NIR laser irradiation, ALP release rates of MEL-added biomaterials were 1.62 times faster than those of MEL-non-added biomaterials. In addition, ALP release using an artificial skin was increased by NIR laser irradiation. ALP release from biomaterials followed Fickian diffusion mechanism, while ALP release using an artificial skin followed a non-Fickian diffusion mechanism. Xanthine oxidase inhibitory (%) for MEL-added biomaterials with/without the addition of GL and XL were 47.5%, 61.7%, and 65.1%, respectively.

1. Introduction

Recently, interests in environmental pollution caused by non-degradable plastic materials has increased. A number of studies have been conducted to develop environmentally friendly biodegradable materials as substitutes for synthetic polymer materials. Biodegradable materials can be rapidly degraded by microorganisms. Synthetic polymers are produced by chemical synthesis while natural polymers are produced by microbial synthesis.

Natural biodegradable polymers include starch, chitosan, alginate, gelatin, cellulose, and so on [1–3]. Of these natural biodegradable polymers, starch is one possible candidate for preparing functional biomedical materials because of its excellent biocompatibility, renewable resources, low cost, and abundance in natural [4–6].

Starch-based functional biomedical materials can be used for wound dressings, carriers for drug delivery, cell drug delivery, transdermal drug delivery system (TDDS), encapsulating agents, cell immobilization, and so forth because they have features such as inherent biodegradability, biocompatibility, and non-toxicity [7–11].

Of various drug delivery systems, TDDS has advantages of improving drug bioavailability, reducing systemic toxicity, and decreasing pain than other of drug delivery systems (oral drug delivery or hypodermic injection) by delivering drugs directly to a local area [12–14]. However, TDDS has limitations in its use because the skin acts as a natural protective barrier. In addition, low molecular weight drugs with high hydrophilicity have a disadvantage in that it is challenging for them to be absorbed through the stratum corneum. Therefore, it is necessary to develop a TDDS to solve this limitation [15–18]. An increase in the degree of absorption of drug using the functional material and an improvement in the degree of penetration using modified drug incorporated formulation are essential factors for solving these problems. Therefore, various studies are in progress to deliver a therapeutic amount of drug to the specific target site in the body and to maintain the constant drug concentration using electrically-responsive copolymers or stimulus-responsive functional materials for TDDS. In case of electrically-responsive copolymers, they are mainly applied in TDDS using poly(acrylamide)-*graft*-pullulan copolymer, poly(acrylamide)-*grafted*-chondroitin, polyacrylamide-*grafted*-gum ghatti copolymer, etc. [19–22]. In addition, functional materials that are stimulus-responsive such as melanin (MEL), peflourhexane, proxamer, and poly(N-isopropylacrylamid) are attracting attention in biomedical applications [23–25]. Among various functional materials, the melanin (MEL)

* Corresponding authors.
E-mail addresses: yskim1@jnu.ac.kr (Y.-S. Kim), yunsd03@jnu.ac.kr (S.-D. Yoon).
[1] These authors contributed equally to this work.

https://doi.org/10.1016/j.ijbiomac.2022.04.116
Received 23 July 2021; Received in revised form 27 March 2022; Accepted 16 April 2022
Available online 22 April 2022

is a well-known multifunctional biomaterial that is widely distributed in the natural world. It is produced by various organisms including animals, bacteria, and fungi. MEL has various specific properties such as light-protecting, antibiotics, antimicrobial, antiviral, anti-inflammatory, thermoregulating, and free radical scavenging activities. In addition, MEL can absorb a large range of light from ultraviolet to near infrared (NIR) regions with a good photothermal conversion efficiency [26–28]. Thus, it is widely used in drug delivery system and photothermal therapy (PTT) based on photothermal conversion efficiency [29,30].

In our previous studies, we have prepared nature polymers-based biomaterials imprinted with sulindac (SLD) [31], atenolol (ATN) [32], and arbutin (AR) [3] for a TDDS and reported the characterization and drug release properties of the prepared biomaterials. From these results, it can be confirmed that SLD, ATL, and AR imprinted biomaterials could be applied as TDDS patches. In addition, we have recently prepared functional thermo-sensitive allopurinol (ALP) imprinted biomaterials added poloxamer (PX) as a thermo-sensitive polymer to improve the degree of absorption of drug through the skin [33]. Experimental results have shown that the absorption and release of ALP are enhanced by the addition of PX, verifying that drugs imprinted on TDDS biomaterials can be effectively released by the functional material. Although many studies have been carried out about the effective release of drugs from a TDDS biomaterials using functional polymers or biomedical materials, few studies have been performed utilizing the photothermal conversion efficiency of MEL for functional TDDS. In addition, there were few reports of biodegradable nature polymers-based TDDS biomaterials for the acute treatment.

In this study, in order to enhance the degree of absorption of drugs through the skin for use in an acute therapy, functional ALP incorporated starch-based biomaterials were prepared with the addition of MEL as a photothermal agent. ALP is one of the most effective and well-known medicine for the treatment of gout and hyperuricaemia. The main function of ALP is to inhibit the xanthine oxidaise enzyme, which is a key component in the uric acid pathway. In addition, it can be an effective urate-lowering therapy (ULT) when adequate doses are used. However, side effects such as ALP hypersensitivity syndrome (AHS) and kidney damage can occur when a high dosage is used [34–36].

The main objective of this study was to prepare functional ALP incorporated starch-based biomaterials containing MEL for effective TDDS to treat patients with acute gout. Photothermal conversion efficiencies of the prepared functional biomaterials with NIR laser irradiation and ALP release properties under different pH and temperature with NIR laser irradiation were investigated. In addition, ALP release mechanisms of diffusion (Fickian and non-Fickian diffusion mechanisms) were determined. Especially, ALP release was evaluated using an artificial skin test to evaluate the application of the prepared biomaterials as a TDDS. Moreover, xanthine oxidase (XO) inhibition properties were investigated using ALP solution released from functional ALP incorporated biomaterials.

2. Experimental

2.1. Materials

Mungbean starch (M) was obtained from Chungwon food (Incheon, South Korea). Melanin (MEL), allopurinol (ALP), sodium benzoate (S), polyvinyl alcohol (PVA) (Mw: 89,000-98,000, degree of hydrolysis (DH): 99%), glycerol (GL), xylitol (XL), xanthine, xanthine oxidase microbial (XO), sodium phosphate dibasic, sodium phosphate monobasic, and 3,3′,5,5′-Tetramethylbenzidine (TMB, Insoluble) were purchased from Sigma-Aldrich (St. Louis, MO, USA). Hydrogen tetrachloroaurate (III) tetrahydrate ($HAuCl_4$) was purchased from Duksan (Pharmaceutical Co., Ltd., Korea). Tris-HCl buffer (pH 7.5) was obtained from Thermo Fisher Scientific (Waltham, MA, USA). All other chemicals and materials were commercially available without further purification. Distilled water (DW) was re-distilled after deionization and used in all experiments.

2.2. Preparation of MEL added functional ALP incorporated starch-based biomaterials

MEL-added functional ALP incorporated starch-based biomaterials were prepared by casting method and UV curing process. The PVA solution was prepared by dissolving PVA in hot DW (98 °C). Mungbean starch, sodium benzoate, and plasticizers (GL or XL) were mixed with DW using a kitchen-aid mixer (Anymix, Hyun-woo Star, Seoul, Korea) at 500 rpm for 30 min. The PVA solution and mixed mungbean starch/sodium benzoate/plasticizers were left at 98 °C for 15 min. The mixture was blended to form a homogeneous gel-like solution with a mechanical stirrer (500 rpm) at room temperature for 70 min. After dissolving ALP (0.5 g) as the target drug and MEL (5 mg) in DW (20 mL), the ALP solution was added dropwise for 20 min for uniform incorporation and dispersion in a gel-like solution during the blending process. Compositions for the preparation of functional ALP incorporated biomaterials are shown in Table 1. Bubbles were removed using an aspirator. The gel-like solution was poured on to a pre-warmed (45 °C) Teflon mold (300 × 300 × 1 mm). Water was evaporated from the mold in a ventilated oven at 45 °C for 24 h. Prepared biomaterials were then cured for 30 min using a UV lamp (OSRAM ULTRA-VITALUX, 300 W) at an atmospheric pressure. After the UV curing process, biomaterials were conditioned at 25 °C for one week with a relative humidity (RH) of 55%.

2.3. Characterization of functional biomaterials

Surfaces and cross-sections of prepared functional biomaterials with/without the addition of MEL and ALP were investigated using a field emission scanning electron microscope (FE-SEM) (S-4700, Hitachi, Tokyo, Japan) at an acceleration voltage of 5.0 kV. Fourier transform infrared spectrophotometry (FT-IR) analysis was performed using an FT-IR spectrophotometer (vertex-70, Bruker, Germany) to confirm functional groups of prepared biomaterials with/without the addition of MEL and ALP. In addition, ALP with/without UV irradiation was examined for ^{1}H nuclear magnetic resonance (^{1}H NMR) spectra to verify the stability of ALP by UV irradiation. ^{1}H NMR spectra were recorded on a Varian Unity Inova 500 MHz spectrometer at the Korea Basic Science Institute (KBSI, Gwangju Center, Korea). Samples for NMR analysis were dissolved in DMSO-d_6.

2.4. Tensile strength and elongation properties

Tensile strength (TS) and elongation properties (EP) of prepared functional starch-based biomaterials were investigated using an Instron 6012 testing machine (Norwood, MA, USA). Six dumbbell shaped specimens (ASTM D-412) were obtained by cutting biomaterials. The thickness of each biomaterial was measured at seven places along the test length using a mechanical scanner (Digital thickness gauge "Mitutoyo" Tokyo, Japan) at 20–23 random positions around the prepared biomaterial. The average thickness of specimens was 0.108 ± 0.004 mm. Gauge length and grip distance were 50.0 mm. The crosshead speed was 20 mm/min and the load cell capacity was 250 kg_f. All tests were conducted at 25 °C with RH of 60.0%.

2.5. Photothermal conversion efficiencies of functional starch-based biomaterials

Photothermal conversion efficiencies of functional starch-based biomaterials were determined as follows. Prepared biomaterials (0.10 g) were irradiated with 808 nm NIR laser (LAB808CW-4 W-f400, Laserlab Co., Seoul, Korea) at a power density of 1.5 W/cm^2 for 21.0 min in standard buffer solution (pH 7.0) at room temperature. Temperature change for MEL added biomaterials were monitored every 3 min using an infrared (IR) thermal imaging camera (C2, FLIR System Inc.,

Table 1
Composition of functional ALP incorporated starch-based biomaterials.

Sample name	Mungbean starch (M) (g)	PVA (P) (g)	MEL (wt%)	GL (wt%)	XL (wt%)	Sodium benzoate (S) (wt%)	ALP (g)	DW (g)
MPS	6.0	4.0	–	–	–	3.0	–	100
MPS-ALP	6.0	4.0	–	–	–	3.0	0.5	100
MPSMEL5	6.0	4.0	0.05	–	–	3.0	–	100
MPSMEL10	6.0	4.0	0.10	–	–	3.0	–	100
MPSMEL20	6.0	4.0	0.20	–	–	3.0	–	100
MPSMEL5-ALP	6.0	4.0	0.05	–	–	3.0	0.5	100
MPMEL5GL-ALP	6.0	4.0	0.05	40	–	3.0	0.5	100
MPSMEL5XL-ALP	6.0	4.0	0.05	–	40	3.0	0.5	100

Sweden).

2.6. ALP release properties

ALP release properties of biomaterials were investigated with/without NIR laser irradiation. Functional biomaterials (0.10 g) were immersed in Petri dishes containing 100 mL buffer solutions at different temperature (25.0, 36.5, and 40.0 °C) and pH 5.8. ALP release properties were then evaluated with/without NIR laser irradiation. At predetermined time intervals, 2 mL of the solution was measured using a UV–vis spectrophotometer (OPTIZEN 2120UV, Neogen, Co., Ltd., Korea) at 257.0 nm. In addition, the possibility of the biomaterials as a TDDS was verified by ALP release test using an artificial skin (Neoderm-ED, Tego Science, Inc. Korea). Prepared functional ALP incorporated biomaterials (2.0 × 2.0 cm) were placed on artificial skins mixed agar-based gel at 36.5 ± 0.5 °C with RH of 60.0 ± 0.5%. Agar-based gel was immersed in DW at 25.0 °C for 6 h. After a certain period of time, ALP release was then measured using a UV–vis spectrophotometer.

2.7. In vitro xanthine oxidase inhibitory activity

All ALP release solutions were assayed for in vitro xanthine oxidase inhibitory (XOI) activities. XOI activity was assayed spectrophotometrically under aerobic conditions using xanthine as a substrate [37–39]. The assay mixture consisted of 1 mL of ALP release solution, 2.9 mL of phosphate buffer solution (pH 7.4), and 0.1 mL of xanthine oxidase (XO) solution (0.01 units/mL in phosphate buffer solution, pH 7.4). After pre-incubation at 25 °C for 15 min, the reaction was initiated by the addition of 2 mL of xanthine solution (150 μM in phosphate buffer solution, pH 7.4). The assay mixture was incubated at 25 °C for 30 min. The reaction was then stopped by the addition of 1 mL of 1 N HCl and its absorbance was measured at 290 nm using a UV–vis spectrophotometer. ALP is one of the most well-known inhibitors of XO. It was used as a positive control in this study. One unit of XO was defined as the amount of enzyme required to produce 1 mmol of uric acid/min at 25 °C. XOI activity was expressed as inhibition (%) of XO in the above assay system. It was calculated as:

$$\text{Inhibition}\ (\%) = \left\{ \frac{(A-B)-(C-D)}{(A-B)} \right\} \times 100 \quad (1)$$

where A was the activity of the enzyme without the ALP release solution, B was the control of A without the ALP release solution and XO solution, C and D were the activities of the ALP release solution with/without XO, respectively.

The inhibitory effect of uric acid synthesis for ALP solution released on functional ALP incorporated biomaterials was also determined using colorimetric sensing of uric acid [40]. XOI activity assay mixtures and 0.05 mM $HAuCl_4$ solution were mixed in tris-HCl buffer (pH 7.5) and incubated at room temperature for 10 min. Then, 0.1 mM TMB solution was added into the above reaction solution. The mixture was vortexed thoroughly at room temperature for 2 min.

2.8. Statistical analysis

All experimental results are presented as mean ± standard deviation (SD). Data of this study were tested for statistical significance using Student's *t*-test through repeated experiments.

3. Results and discussion

3.1. Characterization

To verify the surface and cross-sections characteristics of prepared functional starch-based biomaterials with/without the addition of MEL, the analyses were performed using FE-SEM. Fig. 1 shows SEM images of prepared functional ALP incorporated biomaterials with/without the addition of ALP, MEL, and plasticizers (GL or XL). Results indicated that there was no noticeable agglomeration, voids, porosity, or cracks in SEM images of prepared functional biomaterials except for biomaterials added with 0.10 or 0.20 wt% MEL (Fig. 1c and d). Based on these results, functional ALP incorporated biomaterials were prepared by adding 0.05 wt% MEL.

FT-IR and ^{1}H NMR analyses of ALP before and after UV irradiation were performed to confirm the stability of ALP by UV irradiation for 30 min which was the same preparation condition for ALP incorporated starch-based biomaterials. Fig. 2a and b shows FT-IR spectra and ^{1}H NMR of ALP before and after UV irradiation, respectively. Results indicated that the change of chemical structure for ALP did not change at the synthesis condition after UV irradiation of the biomaterials. FT-IR spectra of characteristic peaks of ALP showed bands at 3066.15 and 2851.19 cm^{-1} for N—H stretching vibrations, 1710.33 cm^{-1} for C═O stretching vibrations, and 1593.67 cm^{-1} for C═C stretching vibrations (see Fig. 2a) [41,42]. In addition, ^{1}H NMR spectra showed characteristic peaks of ALP appeared at 8.03 and 7.96 ppm for protons including chemical structure for ALP (see Fig. 2b) [43]. Furthermore, FT-IR spectra of MEL showed no change due to UV irradiation because the characteristic peaks of MEL appeared at 3411.45 cm^{-1} due to O—H or N—H stretching vibrations, 1716.07 cm^{-1} due to COOH stretching, 1615.97 cm^{-1} due to C═C stretching, and 1398.51 cm^{-1} due to aliphatic C—H stretching [44,45].

Fig. 2b shows FT-IR spectra of functional starch-based biomaterials with/without the addition of ALP and MEL. In the spectra of non-incorporated biomaterials, absorption bands between 845.0 and 912.3 cm^{-1} could be assigned to -C-O-C- ring vibration in granular starch. In addition, absorption bands at 1100.5 and 1005.9 cm^{-1} corresponding to the anhydroglucose ring of starch were observed. Broad absorption bands at 3189.74 and 3170.38 cm^{-1} as asymmetry and symmetry stretching were attributed to hydrogen bonded hydroxyl groups (-OH) [46]. Characteristic peaks of ALP and MEL were appeared at 1585.41 and 1664.27 cm^{-1}. These results of FT-IR analysis for functional ALP incorporated biomaterials with/without the addition of plasticizers (GL or XL), ALP, and MEL verified the presence of characteristic peaks of ALP and MEL. However, other peaks could not be confirmed because of overlapping peaks with similar chemical bonds. Results indicated that functional starch-based biomaterials were successfully prepared by the addition of ALP and MEL.

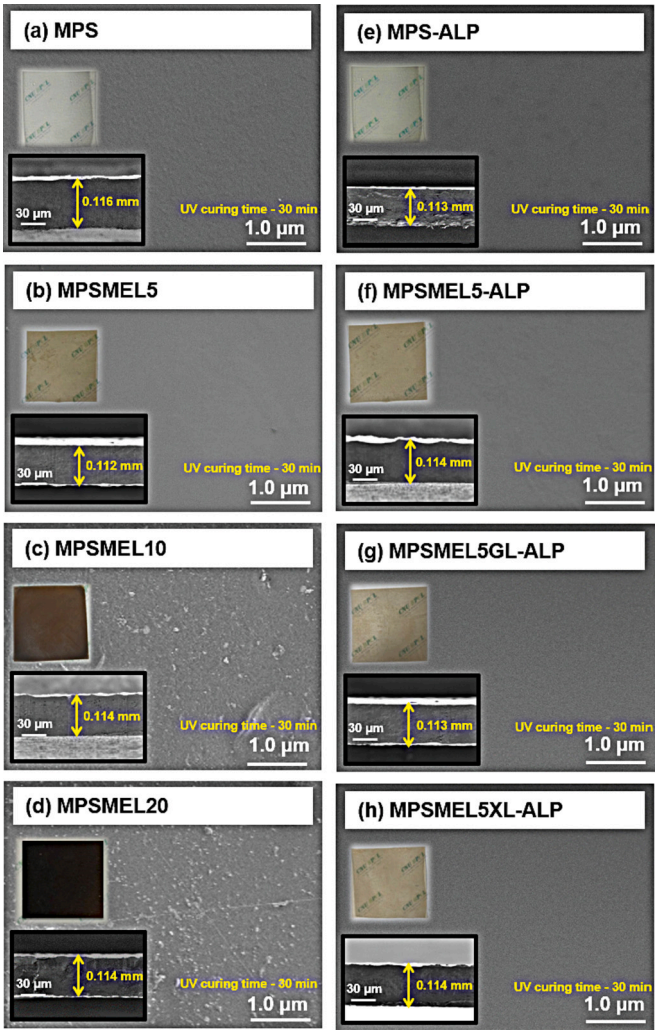

Fig. 1. SEM image (surfaces and cross-sections) of functional ALP incorporated starch-based biomaterials. (a) non-incorporated biomaterial. (b-d) functional non-incorporated biomaterials with MEL contents. (e) ALP incorporated biomaterial. (f) functional ALP incorporated biomaterial. (g-h) functional ALP incorporated biomaterial with the addition of plasticizers.

3.2. Mechanical properties

Evaluating the tensile strength (TS) and elongation properties (EP) as mechanical properties of natural polymer based-biomaterials is necessary to apply them in a TDDS as biomedical materials. Therefore, TS and EP values of functional biomaterials were investigated in this study. Results of TS and EP for the prepared functional biomaterials with/without the addition of ALP, MEL, and plasticizers (GL and XL) are shown in Table 2. The results of TS and EP of MEL-added biomaterial were similar to those of biomaterials without the addition of MEL. In case of GL or XL added functional biomaterials added with MEL, TS values of functional biomaterials without the addition of GL or XL were higher than those of GL or XL-added functional biomaterials, whereas EP values were higher than those of functional biomaterials without the addition of GL or XL. These results confirmed that there was no significant difference in TS or EP as mechanical properties. In addition, differences of mechanical properties did not appear significantly influenced by the addition of ALP in MEL-added biomaterials.

3.3. Photothermal conversion efficiency

To determine photothermal effects after the addition of MEL as a photothermal agent, photothermal conversion efficiencies of MEL-added functional starch-based biomaterials after NIR laser irradiation were investigated. Fig. 3 shows temperature changes of functional biomaterials with/without the addition of MEL and plasticizers under NIR laser irradiation at room temperature. As shown in Fig. 3a, the temperature of biomaterial without the addition of MEL (MPS-ALP) was slightly increased from 26 °C to 29 °C, whereas the temperature of MEL added biomaterial (MPSMEL5-ALP) was drastically increased from 26 °C to 36.8 °C after NIR laser irradiation for 21 min. For ALP incorporated biomaterials added with MEL and GL-added biomaterials (MPSMEL5GL-ALP) or XL-added biomaterials (MPSMEL5XL-ALP), temperatures were increased from 26 °C to 40.1 or 41.5 °C, respectively, after NIR laser irradiation for 21 min (see Fig. 3b). The reason why the temperature of GL or XL added functional biomaterials was higher than that of functional biomaterial without the addition of GL or XL was because many functional groups (hydroxyl groups) present in GL and XL could absorb NIR laser and cause inter-intramolecular interactions. These results confirmed that the addition of MEL to biomaterials under a NIP laser irradiation had photothermal conversion effects. Akomeah et al. [47] have reported that that the suitable temperature of biomaterial is between 40 and 42 °C to apply the biomaterial as a TDDS. These results suggest that the prepared MEL-added biomaterials can be applied as functional biomaterials in a TDDS. Although it is necessary the NIR irradiation for drug release in short time, it can be said to be the effective functional biomaterial for acute treatment in various diseases.

3.4. ALP release properties

ALP release test of functional ALP incorporated starch-based biomaterials was performed to determine their applications in a TDDS to treat gout and hyperuricemia. Fig. 4 shows ALP release profiles of functional ALP incorporated biomaterials with/without the NIR laser irradiation at pH 5.8 and 36.5 °C. The ALP release mechanism was further investigated using Fickian diffusion model and Empirical model for systematic analysis of ALP release behavior. The Fickian diffusion model is generally used for predicting absorption or adsorption behavior of target chemicals due to its simplicity and mathematical manageability. It was obtained using Fick's diffusion on a thin film slab of thickness as shown in the following Eq. (2) [48,49]:

$$\frac{\partial C}{\partial t} = D\frac{\partial^2 C}{\partial x^2} \tag{2}$$

where C was the concentration at time t and D was the constant diffusion coefficient. The solution of Eq. (2) rearranged by the form of a trigonometric series was known as the Fickian diffusion model (3).

$$\frac{M_t}{M_\infty} = 1 - \sum_{n=0}^{\infty} \frac{8}{(2n+1)^2 \bullet \pi^2} \, exp\left[-\frac{D_e \bullet (2n+1)^2 \bullet \pi^2}{l^2} \bullet t \right] \tag{3}$$

where M_t was the amount of drug release at time t, M_∞ was the amount of drug release at infinite time, and l, t, and D_e were the half-thickness of slab, the diffusion time, and the diffusion coefficient, respectively.

The non-Fickian model was represented by the following empirical relation (4).

$$\frac{M_t}{M_\infty} = kt^n \tag{4}$$

where k was the drug release constant and n was the diffusional exponent in terms of the drug release mechanism. In case of $n = 0.5$, the release behavior was a Fickian diffusion mechanism or case I, while $n < 0.5$ was a pesudo-Fickian diffusion mechanism. In addition, $0.5 < n < 1.0$ would indicate a non-Fickian diffusion mechanism (anomalous) while $n \geq 1$ follows case II ($n = 1$) or super case II [50].

Fig. 4 shows results of ALP release for functional ALP incorporated starch-based biomaterials with/without the addition of MEL and

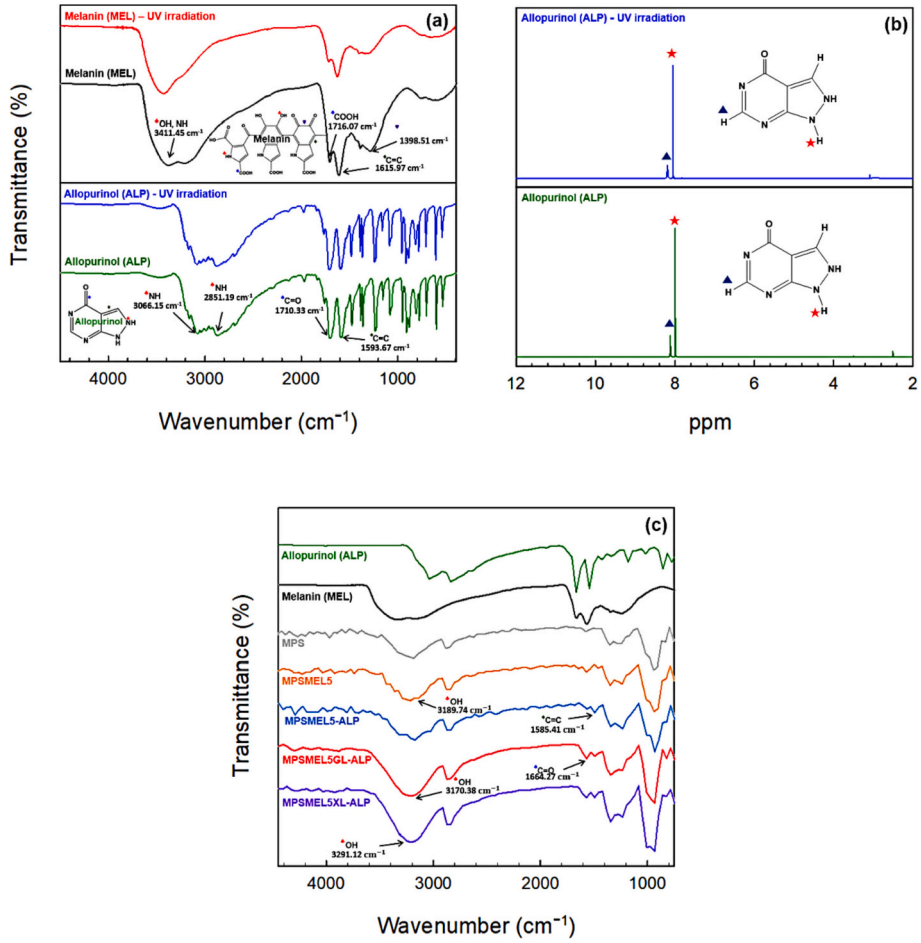

Fig. 2. FT-IR spectra of MEL and ALP with/without UV irradiation (a), ^{1}H NMR of ALP with/without UV irradiation (b), and functional ALP incorporated starch-based biomaterials with/without the addition of ALP, MEL, and plasticizers (GL and XL) (c).

Table 2
Mechanical properties of functional ALP incorporated starch-based biomaterials.

Sample name	Tensile strength (MPa)	Elongation at break (%)
MPS	70.8 ± 1.84	13.3 ± 1.04
MPS-ALP	72.7 ± 1.77	12.7 ± 1.10
MPSMEL5	73.2 ± 1.98	12.9 ± 1.27
MPSMEL5-ALP	73.7 ± 1.69	11.9 ± 1.19
MPSMEL5GL	20.67 ± 1.08	105.7 ± 3.51
MPSMEL5GL-ALP	25.12 ± 1.15	99.55 ± 2.47
MPSMEL5XL	18.75 ± 0.89	108.9 ± 3.83
MPSMEL5XL-ALP	23.85 ± 1.02	102.8 ± 2.97

plasticizers under human skin conditions (pH 5.8 and 36.5 °C) during NIR laser irradiation. As shown in Fig. 4a, ALP release rates of ALP incorporated biomaterials without the addition of MEL and plasticizers were almost similar (at 51.7% and 53.8%, respectively) regardless of NIR laser irradiation. These results were verified by an ALP release rate of 3.49E-11 m^2/s for MPS-ALP with NIR irradiation and an ALP release rate of 3.631E-11 m^2/s for MPS-ALP with NIR irradiation (see Table 3).

Fig. 4b shows the ALP release rates (%) of MEL-added functional ALP incorporated starch-based biomaterials (MPSMEL5-ALP) with/without NIR laser irradiation under pH 5.8 and 36.5 °C. The ALP release rate was 84.8% for MPSMEL5-ALP with NIP laser irradiation within 21 min, whereas it was 52.3% without NIP laser irradiation. The ALP release rate with NIR irradiation (1.09E-10 m^2/s) also tended to be faster than that without NIR irradiation (3.78E-11 m^2/s). These results indicated that ALP release (%) from MPSMEL5-ALP with NIR laser irradiation was 1.62 times faster than that without NIR laser irradiation. These results verified that the degree of ALP release (%) was increased by the addition of MEL to ALP incorporated biomaterials due to its photothermal conversion effects. ALP release (%) results for ALP incorporated biomaterials added with MEL and plasticizers (GL and XL) upon NIR laser irradiation are shown in Fig. 4c. ALP release rates (%) of MPSMEL5XL-ALP and MPSMEL5GL-ALP with NIR laser irradiation were more than 99.0% within 21 min. These results and Table 3 revealed that there were significant differences in ALP release under NIR laser irradiation depending on plasticizers added to functional ALP incorporated biomaterials. ALP release showed the following order: MPSMEL5XL-ALP (3.25E-10 m^2/s) > MPSMEL5GL-ALP (2.49E-10 m^2/s) > MPSMEL5-ALP (1.09E-10 m^2/s). Such high ALP release rates (%) of ALP incorporated biomaterials added with MEL and plasticizers were due to their better photothermal conversion efficiencies than functional ALP incorporated biomaterials without the addition of plasticizers. As shown in the results of Fig, 3, photothermal conversion efficiencies of plasticizers and MEL-added biomaterials were better than that of MEL-added biomaterials without the addition of plasticizers. Therefore, it is considered that the degree of ALP release was improved by the temperature increase of MEL-added biomaterials and the changes of structure between components of biomaterials. As shown in Fig. 4 (line) and Table 3, the results indicated that the ALP release behavior of Fickian diffusion model using the buffer solution was more satisfactory than that of the empirical model. In addition, the diffusional exponent (n) of functional ALP incorporated biomaterials calculated by the empirical model was less than 0.5, clearly indicating that ALP release behavior followed the pesudo-Fickian diffusion mechanism.

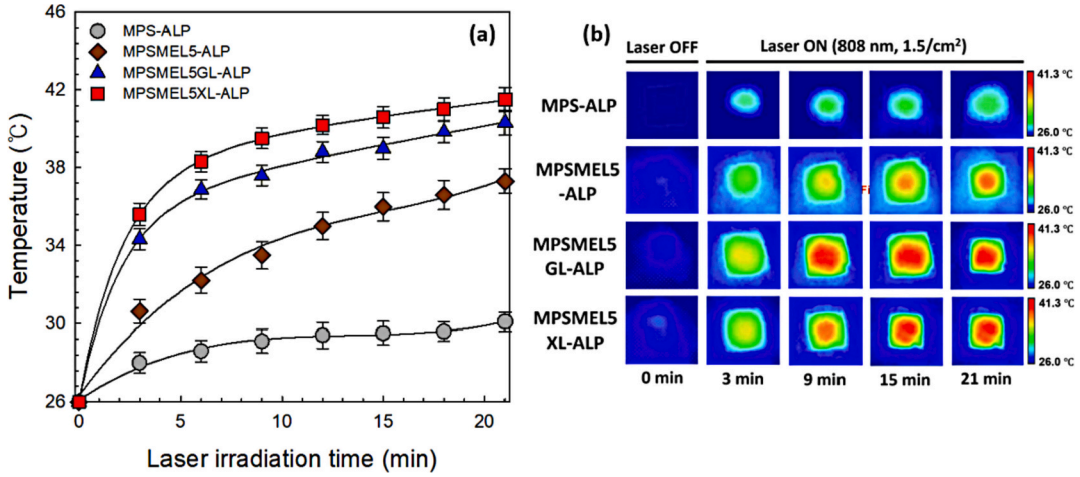

Fig. 3. (a) Photothermal heating curve of functional ALP incorporated starch-based biomaterials with/without the addition of MEL and plasticizers under 808 NIR laser irradiation at 1.5 W/cm^2 for 21 min. (b) IR thermal image of functional ALP incorporated biomaterials with/without the addition of MEL and plasticizers under 808 NIR laser irradiation at 1.5 W/cm^2 for 21 min.

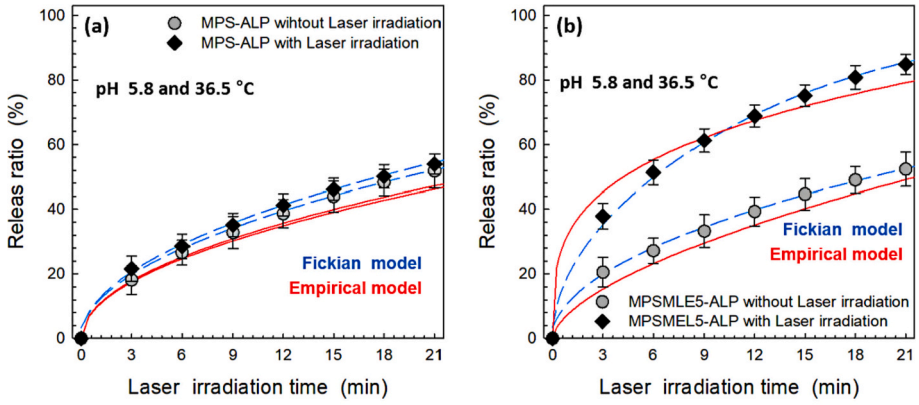

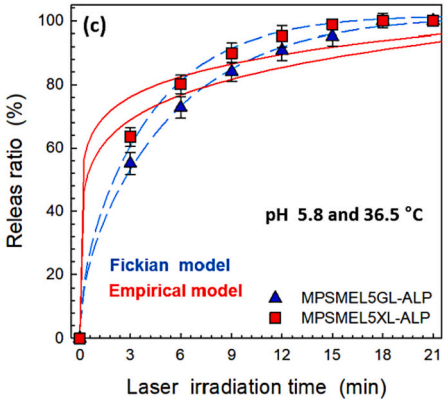

Fig. 4. Experimental and diffusion model fits of ALP release (%) from functional ALP incorporated starch-based biomaterials with/without 808 NIR laser irradiation in buffer solution. (a) ALP release (%) from MEL non-added biomaterial with/without NIR laser irradiation at pH 5.8 and 20 °C. (b) ALP release (%) from MEL added biomaterial with/without NIR laser irradiation at pH 5.8 and 36.5 °C. (c) ALP release (%) from MEL added biomaterial with the addition of plasticizers by NIR laser irradiation at pH 5.8 and 36.5 °C.

3.5. ALP release properties using artificial skin

To confirm the applicability of functional ALP incorporated starch-based biomaterials as a TDDS, ALP release experiment was carried out using artificial skin under human skin conditions (pH 5.8, 36.5 °C and RH 58.0%).

Fig. 5 shows ALP release profiles of functional ALP incorporated starch-based biomaterials using artificial skin. Cumulative release rates of ALP from functional ALP incorporated biomaterials were increased at a relatively constant ratio with increasing of NIR laser irradiation time. The ALP release rate (%) and ALP release behavior for MPSMEL5-ALP with/without NIR laser irradiation using artificial skin are shown in Fig. 5a. The cumulative release rate of ALP without NIR laser irradiation was 18.0% for 21 min, whereas it was increased to 38.9% with NIR laser irradiation. These results confirmed that the degree of ALP release (%) increased by photothermal conversion efficiency of MEL added to biomaterials under artificial skin test. When compared with buffer solution and artificial skin test for ALP release (%), ALP release (%) at buffer

Table 3
Fickian diffusion and empirical model parameters of ALP release from functional ALP incorporated starch-based biomaterials with/without NIR laser irradiation using standard buffer solution.

	MPS-ALP with NIR laser	MPS-ALP without NIR laser	MPSMEL5-ALP with NIR laser	MPSMEL5-ALP without NIR laser	MPSMEL5 GL-ALP	MPSMEL5 XL-ALP
Fickian diffusion model						
M_∞	51.3842	53.7815	54.1682	83.8915	101.8001	101.9280
De	3.49E-11	3.631E-11	3.78E-11	1.09E-10	2.49E-10	3.25E-10
R^2	0.998	0.999	0.998	0.997	0.998	0.997
Empirical model						
M_∞	14.1315	15.7171	19.3014	46.6882	68.3029	71.0330
k	0.6413	0.9695	0.4097	0.7082	0.8169	1.404
n	0.4325	0.3804	0.3522	0.2866	0.1557	0.1172
R^2	0.880	0.898	0.901	0.869	0.790	0.757

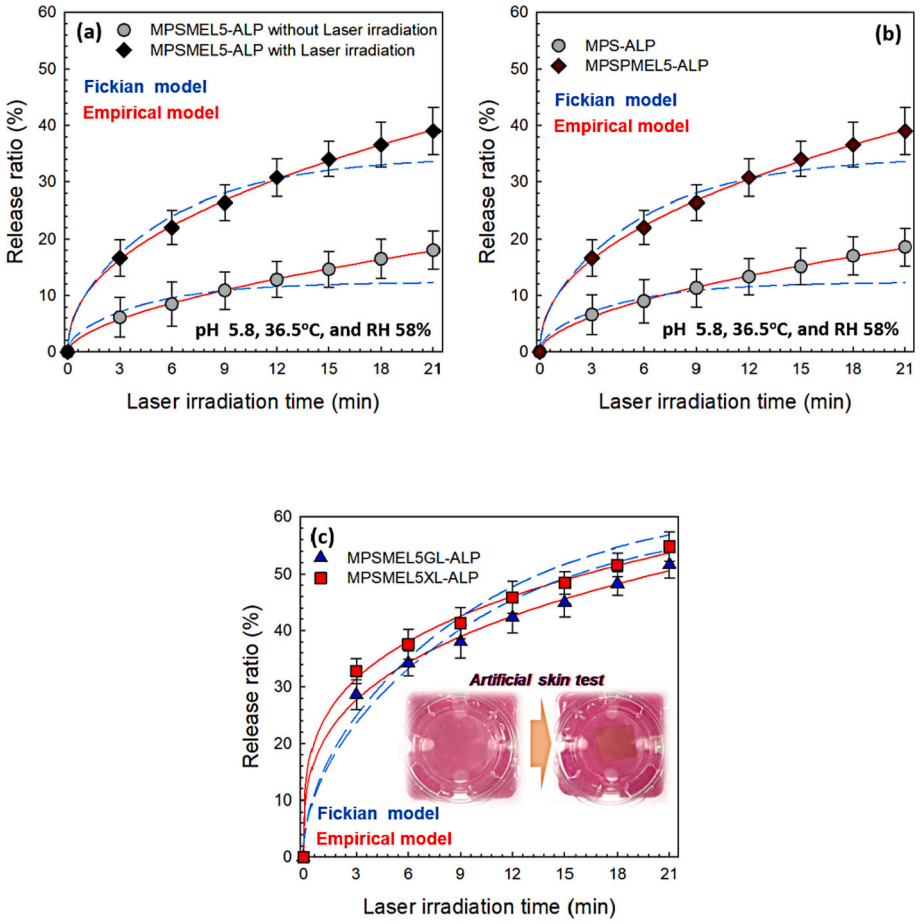

Fig. 5. Experimental and diffusion model fits of ALP release (%) from functional ALP incorporated starch-based biomaterials with/without 808 NIR laser irradiation using artificial skin (pH 5.8, 36.5 °C, and RH 58%). (a) ALP release (%) from MEL added biomaterial with/without NIR laser. (b) ALP release (%) from biomaterials with/without the addition of MEL by NIR laser irradiation. (c) ALP release (%) from MEL added biomaterial with the addition of plasticizers by NIR laser irradiation.

solution was about 2.2 times higher than that of at artificial skin test. It is considered that the reason is ALP is released from all parts of the prepared biomaterials at buffer solution. Fig. 5b and c presents results of ALP release rate (%) and ALP release behavior for functional ALP incorporated biomaterials with/without the addition of MEL and plasticizers (GL and XL) under NIR laser irradiation. Degrees of ALP release from functional ALP incorporated biomaterials depending on the addition of MEL and plasticizers were found to have the following order: MPSMEL5XL-ALP > MPSMEL5GL-ALP > MPSMEL5-ALP > MPS-ALP. In addition, as shown in Fig. 5 (line) and Table 4 (n value), the ALP release (%) using artificial skin determined by the empirical model was more satisfactory than that by the Fickian diffusion model. ALP release mechanism also followed a non-Fickian diffusion mechanism because n value was calculated by the empirical model as a value greater than 0.5. These results suggest that MEL-added biomaterials with NIR laser irradiation as a TDDS can be used for therapy of acute gout and a drug release control.

3.6. *In vitro xanthine oxidase inhibitory activity*

Xanthine oxidase (XO) is the main enzyme required to produce uric acid by the degradation of purine nucleotide in the body. Thus, xanthine oxidase inhibitory (XOI) plays the most important role in the treatment of gout [51]. In order to verify the applicability of the prepared

Table 4
Fickian diffusion and empirical model parameters of ALP release from functional ALP incorporated starch-based biomaterials with/without NIR laser irradiation using artificial skin at pH 5.8, 36.5 °C, and RH 58%.

	MPSMEL5-ALP without NIR laser	MPSMEL5-ALP	MPS-ALP	MPSMEL5 GL-ALP	MPSMEL5 XL-ALP
Fickian diffusion model					
M_∞	12.3242	34.5046	51.3842	60.6015	62.9271
De	1.02E-11	6.27E-11	1.27E-11	1.38E-10	1.43E-10
R^2	0.907	0.912	0.889	0.909	0.897
Empirical model					
M_∞	3.5557	20.4144	10.4929	26.5244	32.3049
k	0.8575	0.4887	0.3202	0.7426	0.7204
n	0.5814	0.5482	0.5685	0.5305	0.5233
R^2	0.999	0.999	0.998	0.997	0.998

functional ALP incorporated starch-based biomaterials for gout treatment as a TDDS, the XOI test was performed using xanthine as the substrate in the present study. Fig. 6a shows results of XOI activity of ALP released into a solution from ALP incorporated biomaterials with/without the addition of MEL and plasticizers according to NIR laser irradiation time. The XOI activity (%) tended to increase with an increase in NIR laser irradiation time. XOI activities (%) of functional ALP incorporated biomaterials with the addition of plasticizers (MPSMEL5GL-ALP and MPSMEL5XL-ALP) were about 2.5 times higher than those of ALP incorporated biomaterial without the addition of MEL or plasticizers (MPS-ALP). The XOI activities (%) of the prepared functional ALP incorporated biomaterials were as follows: MPS-ALP, 26.3%; MPSMEL5-ALP, 47.5%; MPSMEL5GL-ALP, 61.7%; and MPSMEL5XL-ALP, 65.1%.

Colorimetric sensing of uric acid test was also performed using chromogenic reaction of TMB and $HAuCl_4$ to verify the inhibitory effect of uric acid synthesis for ALP released to solution from functional ALP incorporated starch-based biomaterials (Fig. 6b). $HAuCl_4$ can catalyze the oxidation of TMB in the presence of ALP with color changes from colorless to blue oxidized TMB (ox-TMB). However, the reaction does not proceed in the presence of uric acid [40]. As shown in Fig. 6b, the non-treatment group appeared colorless due to the present of uric acid, whereas there was a color change (appeared in blue color) for XOI assay mixture group treated with ALP. In addition, there was a color change in saturation with an increase of ALP release, showing the following increasing order: MPSMEL5XL-ALP > MPSMEL5GL-ALP > MPSMEL5-ALP > MPS-ALP. These results indicated that the prepared functional ALP incorporated biomaterials had excellent effects as XO inhibitors. Therefore, the prepared functional ALP incorporated biomaterials could be used in a TDDS to treat gout.

4. Conclusions

Functional allopurinol (ALP) incorporated biomaterials using mungbean starch, PVA, MEL, and plasticizers (GL and XL) were successfully synthesized using a UV curing process and a casting methods. Photothermal conversion efficiencies of functional ALP incorporated biomaterials were investigated under 808 NIR laser irradiation at 1.5 W/cm^2. Results indicated that the temperature changes of MEL-added biomaterials were about 1.27 times higher than those of biomaterials without the addition of MEL. To confirm the applicability of functional ALP incorporated biomaterials in a TDDS, their ALP release properties were determined with/without NIR laser irradiation. ALP release rate (%) of MEL-added ALP incorporated biomaterials under NIR laser irradiation at pH 5.8 and 36.5 °C were 1.62 times faster than those without NIR laser irradiation. These results confirmed that the degree of ALP release (%) was increased by the addition of MEL due to its photothermal conversion efficiency. In addition, ALP release mechanism

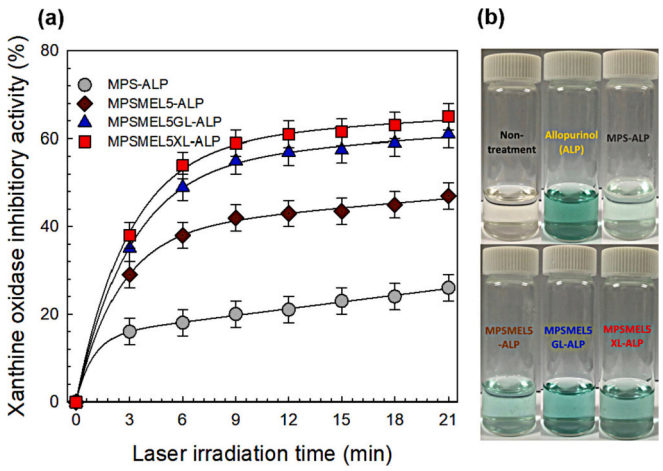

Fig. 6. (a) in vitro xanthine oxidase inhibitory (XOI) activity of ALP release solutions for functional ALP incorporated starch-based biomaterials with/without the addition of MEL and plasticizers by 808 NIR laser irradiation. (b) Photographs of colorimetric sensing of uric acid test for different ALP release solutions treated XOI assay mixtures.

calculated by Fickian diffusion and empirical models verified that the ALP release behavior could be satisfactorily explained by the pseudo-Fickian diffusion mechanism. Likewise, in case of ALP release (%) using an artificial skin, the ALP release was increased at a relatively steady-state rate with increasing NIR laser irradiation time. In addition, ALP release mechanism was explained by empirical models, showing that the ALP release (%) mechanism in the artificial skin test followed the non-Fickian diffusion mechanism. Xanthine oxidase inhibitory (XOI) activity test of ALP solution released from ALP incorporated biomaterials with the addition of MEL and plasticizers (GL and XL) under NIR laser irradiation time on was about 2.5 times higher than that of ALP solution released from ALP incorporated biomaterial without the addition of MEL or plasticizers. Colorimetric sensing of uric acid test was also conducted using chromogenic reaction of TMB and $HAuCl_4$. Results indicated that the non-treatment group appeared colorless due to the presence of uric acid, whereas the color changed (appeared in blue color) in the XOI assay mixture group treated with ALP. These results suggest that functional ALP incorporated biomaterials could be applied to a TDDS for therapy acute gout patients.

Acknowledgments

This research was supported by Basic Science Research Program through the National Research Foundation of Korea (NRF) funded by the Ministry of Education (Grant no. NRF- 2019R1I1A3A01061508).

References

[1] S.H. Hsu, K.C. Hung, C.E. Chen, Biodegradable polymer scaffolds, J. Mater. Chem. B 4 (47) (2016) 7493–7505.
[2] F.F. Azhar, A. Olad, A. Mirmohseni, Development of novel hybrid nanocomposites based on natural biodegradable polymer–montmorillonite/polyaniline: preparation and characterization, Polym. Bull. 71 (7) (2014) 1591–1610.
[3] H.S. Kim, K.J. Kim, M.W. Lee, S.Y. Lee, Y.H. Yun, W.G. Shim, S.D. Yoon, Preparation and release properties of arbutin imprinted inulin/polyvinyl alcohol biomaterials, Int. J. Biol. Macromol. 161 (2020) 763–770.
[4] N. Reddy, Y. Yang, Citric acid cross-linking of starch films, Food Chem. 118 (3) (2010) 702–711.
[5] L.S. Nair, C.T. Laurencin, Biodegradable polymers as biomaterials, Prog. Polym. Sci. 32 (8–9) (2007) 762–798.
[6] Y.N. Sudhakar, M. Selvakumar, D.K. Bhat, LiClO4-doped plasticized chitosan and poly (ethylene glycol) blend as biodegradable polymer electrolyte for supercapacitors, Ionics 19 (2) (2013) 277–285.
[7] B.V. Bochove, D.W. Grijpma, Photo-crosslinked synthetic biodegradable polymer networks for biomedical applications, J. Biomater. Sci. Polym. Ed. 30 (2) (2019) 77–106.

[8] M. Alizadeh-Osgouei, Y. Li, C. Wen, A comprehensive review of biodegradable synthetic polymer-ceramic composites and their manufacture for biomedical applications, Bioact. Mater. 4 (2019) 22–36.
[9] I.J. Macha, B. Ben-Nissan, J. Santos, S. Cazalbou, A. Stamboulis, D. Grossin, G. Giordano, Biocompatibility of a new biodegradable polymer-hydroxyapatite composite for biomedical applications, J. Drug Deliv. Sci. Technol. 38 (2017) 72–77.
[10] J. Park, J.K. Kim, S.J. Patil, J.K. Park, S. Park, D.W. Lee, A wireless pressure sensor integrated with a biodegradable polymer stent for biomedical applications, Sensors 16 (6) (2016) 809.
[11] S. Kumar, S. Raj, S. Jain, K. Chatterjee, Multifunctional biodegradable polymer nanocomposite incorporating graphene-silver hybrid for biomedical applications, Mater. Des. 108 (2016) 319–332.
[12] S. Babaie, A.R.D. Bakhshayesh, J.W. Ha, H. Hamishehkar, K.H. Kim, Invasome: a novel nanocarrier for transdermal drug delivery, Nanomaterials 10 (2) (2020) 341.
[13] P. Desai, R.R. Patlolla, M. Singh, Interaction of nanoparticles and cell-penetrating peptides with skin for transdermal drug delivery, Mol. Membr. Biol. 27 (7) (2010) 247–259.
[14] D. Park, H. Park, J. Seo, S. Lee, Sonophoresis in transdermal drug deliverys, Ultrasonics 54 (1) (2014) 56–65.
[15] K.B. Ita, Transdermal drug delivery: progress and challenges, J. Drug Deliv. Sci. Technol. 24 (3) (2014) 245–250.
[16] K. Ita, Dissolving microneedles for transdermal drug delivery: advances and challenges, Biomed. Pharmacother. 93 (2017) 1116–1127.
[17] B.C.Q. Seah, B.M. Teo, Recent advances in ultrasound-based transdermal drug delivery, Int. J. Nanomedicine 13 (2018) 7749.
[18] M. Singhal, M. Lapteva, Y.N. Kalia, Formulation challenges for 21st century topical and transdermal delivery systems, Expert Opin. Drug Deliv. 14 (6) (2017) 705–770.
[19] S.B. Patil, S.Z. Inamdar, K.K. Das, K.G. Akamanchic, A.V. Patild, A.C. Inamadar, K. R. Reddy, A.V. Raghu, R.V. Kulkarni, Tailor-made electrically-responsive poly (acrylamide)-graft-pullulan copolymer based transdermal drug delivery systems: synthesis, characterization, in-vitro and ex-vivo evaluation, J. Drug Deliv. Sci. Technol. 56 (2020), 101525.
[20] S.B. Patil, S.Z. Inamdar, K.R. Reddy, A.V. Raghu, S.K. Soni, R.V. Kulkarni, Novel biocompatible poly(acrylamide)-grafted-dextran hydrogels: synthesis, characterization and biomedical applications, J. Microbiol. Methods 159 (2019) 200–210.
[21] S.B. Patil, S.Z. Inamdar, K.R. Reddy, A.V. Raghu, K.G. Akamanchi, A.C. Inamadar, K.K. Das, R.V. Kulkarni, Functionally tailored electro-sensitive poly(acrylamide)-g-pectin copolymer hydrogel for transdermal drug delivery application: synthesis, characterization, in-vitro and ex-vivo evaluation, Drug Deliv. Lett. 10 (2020) 185–196.
[22] L. Xu, Y. Yang, Y. Mao, Z. Li, Self-powerbility in electrical stimulation drug delivery system, Adv. Mater. Technol. 7 (2022), 2100055.
[23] R. Cheng, F. Meng, C. Deng, H.A. Klok, Z. Zhong, Dual and multi-stimuli responsive polymeric nanoparticles for programmed site-specific drug delivery, Biomaterials 34 (14) (2013) 3647–3657.
[24] T. Chen, R. Ferris, J. Zhang, R. Ducker, S. Zauscher, Stimulus-responsive polymer brushes on surfaces: transduction mechanisms and applications, Prog. Polym. Sci. 35 (1–2) (2010) 94–112.
[25] L. Zhai, Stimuli-responsive polymer films, Chem. Soc. Rev. 42 (17) (2013) 7148–7160.
[26] P. Yang, S. Zhang, N. Zhang, Y. Wang, J. Zhong, X. Sun, Y. Qi, X. Chen, Z. Li, Y. Li, Tailoring synthetic melanin nanoparticles for enhanced photothermal therapy, ACS Appl. Mater. Interfaces 11 (45) (2019) 42671–42679.
[27] Y. Ye, C. Wang, X. Zhang, Q. Hu, Y. Zhang, Q. Liu, D. Wen, J. Milligan, A. Bellotti, L. Huang, G. Dotti, Z. Gu, A melanin-mediated cancer immunotherapy patch, Sci. Immunol. 2 (17) (2017).
[28] M.A. Kim, S.D. Yoon, E.M. Kim, H.J. Jeong, C.M. Lee, Natural melanin-loaded nanovesicles for near-infrared mediated tumor ablation by photothermal conversion, Nanotechnology 29 (41) (2018), 415101.
[29] Y. Liu, K. Ai, J. Liu, M. Deng, Y. He, L. Lu, Dopamine-melanin colloidal nanospheres: an efficient near-infrared photothermal therapeutic agent for in vivo cancer therapy, Adv. Mater. 25 (9) (2013) 1353–1359.
[30] M.A. Kim, S.D. Yoon, C.M. Lee, A drug release system induced by near infrared laser using alginate microparticles containing melanin, Int. J. Biol. Macromol. 103 (2017) 839–844.
[31] H.Y. Tak, Y.H. Yun, C.M. Lee, S.D. Yoon, Sulindac imprinted mungbean starch/PVA biomaterial films as a transdermal drug delivery patch, Carbohydr. Polym. 208 (2019) 261–268.
[32] H.S. Kim, Y.H. Yun, W.G. Shim, S.D. Yoon, Preparation of atenolol imprinted polysaccharide based biomaterials for a transdermal drug delivery system, J. Drug Deliv. Sci. Technol. 59 (2020), 101893.
[33] H.S. Kim, Y.H. Yun, W.G. Shim, S.D. Yoon, Preparation and evaluation of functional allopurinol imprinted starch based biomaterials for transdermal drug delivery, Int. J. Biol. Macromol. 175 (2021) 217–228.
[34] A.B. Vargas-Santos, C.E. Peloquin, Y. Zhang, Association of chronic kidney disease with allopurinol use in gout treatment, JAMA Intern. Med. 178 (2018) 1526–1533.
[35] M. Iqbal, E. Ezzeldin, R.N. Herqash, O. Alam, Ultra-performance hydrophilic interaction liquid chromatography coupled with tandem mass spectrometry for simultaneous determination of allopurinol, oxypurinol and lesinurad in rat plasma: application to pharmacokinetic study in rats, PloS One 14 (3) (2019), e0213786.
[36] L.K. Stamp, R.O. Day, J. Yun, Allopurinol hypersensitivity: investigating the cause and minimizing the risk, Nat. Rev. Rheumatol. 12 (2016) 235–242.
[37] M. Umamaheswari, K. Asokkumar, A.T. Sivashanmugam, A. Remyaraju, V. Subhadradevi, T.K. Ravi, In vitro xanthine oxidase inhibitory activity of the fractions of Erythrina stricta roxb, J. Ethnopharmacol. 124 (3) (2009) 646–648.
[38] Y.C. Song, H. Li, Y.H. Ye, C.Y. Shan, Y.M. Yang, R.X. Tan, Endophytic naphthopyrone metabolites are co-inhibitors of xanthine oxidase, SW1116 cell and some microbial growths, FEMS Microbiol. Lett. 241 (1) (2004) 67–72.
[39] M. Umamaheswari, K. AsokKumar, A. Somasundaram, T. Sivashanmugam, V. Subhadradevi, T.K. Ravi, Xanthine oxidase inhibitory activity of some indian medical plants, J. Ethnopharmacol. 109 (3) (2007) 547–551.
[40] J. Wang, X. Fang, Y. Zhang, X. Cui, H. Zhao, X. Li, Z. Li, A simple and rapid colorimetric probe for uric acid detection based on redox reaction of 3, 3′, 5, 5′-tetramethylbenzidine with HAuCl4, Colloids Surf. A Physicochem. Eng. Asp. 555 (2018) 565–571.
[41] A. Gerega, L. Lapinski, I. Reva, H. Rostkowska, M.J. Nowak, UV-induced generation of rare tautomers of allopurinol and 9-methylhypoxanthine-a matrix isolation FTIR study, Biophys. Chem. 122 (2006) 123–135.
[42] L. Deng, Y. Lia, F. Feng, D. Wu, H. Zhang, Encapsulation of allopurinol by glucose cross-linked gelatin/zein nanofibers: characterization and release behavior, Food Hydrocoll. 94 (2019) 574–584.
[43] M.S. Refat, G.G. Mohamed, A. Fathi, Spectrophotometric determination of allopurinol drug in tablets: spectroscopic characterization of the solid CT complexes, Bull. Korean Chem. Soc. 31 (6) (2010) 1535–1542.
[44] S. Sajjan, G. Kulkarni, V. Yaligara, K. Lee, T.B. Karegoudar, Purification and physiochemical characterization of melanin pigment from klebsiella sp. GSK, J. Microbiol. Biotechnol. 20 (11) (2010) 1513–1520.
[45] J. Stainsack, A.S. Mangrich, C.M. Maia, V.G. Machado, J.C. dos Santos, S. Nakagaki, Spectroscopic investigation of hard and soft metal binding sites in synthetic melaninm, Inorg. Chim. Acta 356 (2003) 243–248.
[46] A.V. Raghu, G.S. Gadaginamath, M. Priya, P. Seema, H.M. Jeong, T. M. Aminabhavi, Synthesis and characterization of novel polyurethanes based on N1, N4-bis[(4-hydroxyphenyl)methylene]succinohydrazide hard segment, J. Appl. Polym. Sci. 110 (2008) 2315–2320.
[47] F. Akomeah, T. Nazir, G.P. Martin, M.B. Brown, Effect of heat on the percutaneous absorption and skin retention of three model penetrants, Eur. J. Pharm. Sci. 21 (2–3) (2004) 337–345.
[48] E. Celik, I. Guven, E. Madenci, Experimental and numerical characterization of non-fickian moisture diffusion in electronic packages, IEEE Trans. Adv. Packag. 32 (3) (2009) 666–674.
[49] E.M. Davis, M. Minelli, M. Giacinti Baschetti, Y.A. Elabd, Non-fickian diffusidon of water in polylactide, Ind. Eng. Chem. Res. 52 (26) (2013) 8664–8673.
[50] D.A. Winkler, A. Starks, The non-fickian diffusion of deterrents into a nitrocellulose-based propellant, J. Appl. Polym. Sci. 35 (1) (1988) 51–62.
[51] M. Rajesh, P. Mukhopadhyay, S. Bátkai, B. Mukhopadhyay, V. Patel, G. Haskó, C. Szabó, J.G. Mabley, L. Liaudet, P. Pacher, Xanthine oxidase inhibitor allopurinol attenuates the development of diabetic cardiomyopathy, J. Cell. Mol. Med. 13 (8b) (2009) 2330–2341.